

Spin pumping from a ferromagnetic insulator into an altermagnet

Chi Sun and Jacob Linder 

Center for Quantum Spintronics, Department of Physics, Norwegian University of Science and Technology, NO-7491 Trondheim, Norway

 (Received 23 August 2023; revised 2 October 2023; accepted 5 October 2023; published 18 October 2023)

A class of antiferromagnets with spin-polarized electron bands, yet zero net magnetization, called altermagnets, is attracting increasing attention due to their potential use in spintronics. Here, we study spin injection into an altermagnet via spin pumping from a ferromagnetic insulator. We find that the spin pumping behaves qualitatively differently depending on how the altermagnet is crystallographically oriented relative to the interface of the ferromagnetic insulator. The altermagnetic state can enhance or suppress spin pumping, which we explain in terms of the spin-split altermagnetic band structure and the spin-flip probability for the incident modes. Including the effect of interfacial Rashba spin-orbit coupling, we find that the spin-pumping effect is in general magnified, but that it can display a nonmonotonic behavior as a function of the spin-orbit coupling strength. We show that there exists an optimal value of the spin-orbit coupling strength which causes an order of magnitude increase in the pumped spin current, even for the crystallographic orientation of the altermagnet which suppresses the spin pumping.

DOI: [10.1103/PhysRevB.108.L140408](https://doi.org/10.1103/PhysRevB.108.L140408)

Introduction. Spin pumping is a mechanism for generating spin currents in which the precessing magnetization in a magnetic material transfers angular momentum into its adjacent nonmagnetic layers [1–6]. Compared with metals, magnetic insulators can function as efficient spin-current sources with low dissipation and reduced energy loss [4], in which the ferromagnetic insulator (FI) yttrium iron garnet (YIG) demonstrates the lowest known spin dissipation with an exceptionally low Gilbert damping [7,8]. In conventional FI/normal metal (NM) heterostructures, the injected spin current affects the magnetization dynamics in the FI and creates a spin accumulation in the NM, resulting in a measurable damping increase in the linewidth of a ferromagnetic resonance (FMR) signal, which has been extensively investigated [3,9–11]. When the NM is replaced by another material such as a superconductor, the spin-pumping effect is considerably modulated by various superconducting gap properties and interfacial effects [12–19].

Recently, a new magnetic phase dubbed altermagnetism [20–23] has attracted increasing attention. Such materials exhibit a large momentum-dependent spin splitting and vanishing net macroscopic magnetization at the same time, thus combining features from conventional ferromagnets and antiferromagnets [24–27]. The spin splitting in the altermagnet (AM), which is of a strong nonrelativistic origin, is protected by the broken symmetries of the spin arrangements on the crystal, distinct from ferromagnetic and relativistically spin-orbit coupled (SOC) systems [24,25,28]. It is predicted that AM can span a large range of materials, from insulators such as FeF₂ and MnF₂, semiconductors such as MnTe, metals such as RuO₂, to superconductors such as La₂CuO₄ [24,29–31]. These novel properties make AM a fascinating material platform to investigate superconducting [26,32–36] and spintronics phenomena [37–41].

In this Letter, we theoretically determine spin pumping from a FI into a metallic AM in a FI/AM bilayer (see Fig. 1).

To cover different crystallographic orientations of the interface relative to the spin-polarized lobes of the altermagnetic Fermi surface, two representative metallic AMs, as shown in Figs. 1(a) and 1(b), are studied in detail. In addition to the nonrelativistic interfacial effect induced by the AM, a relativistic Rashba SOC is included at the FI/AM interface in our model. We find that the spin-pumping current can be enhanced or suppressed by altermagnetism, depending on the interface orientation, thus offering versatility. This is explained in terms of the spin-split altermagnetic band structure and the spin-flip probability for the incident modes toward the interface. In addition, the spin-pumping current shows a nonmonotonic behavior as a function of the interfacial SOC strength. We show that the interfacial SOC can, in a certain range, increase the spin-pumping current in a FI/AM bilayer by more than an order of magnitude.

Theory. The effective low-energy Hamiltonian for the AM shown in Fig. 1(a), using an electron field operator basis $\psi = [\psi_{\uparrow}, \psi_{\downarrow}]^T$, is given by

$$H_{\text{AM}} = -\frac{\hbar^2 \nabla^2}{2m_e} - \mu + \alpha \sigma_z k_x k_y, \quad (1)$$

in which α is the parameter that characterizes the altermagnetism strength, σ_z denotes the Pauli matrix, m_e is the electron mass, and μ is the chemical potential. By solving the stationary Schrödinger equation as an eigenvalue problem [see Supplemental Material (SM) [42] for details], the x components of the wave vectors in the AM with energy E are given by $k_{e\uparrow(\downarrow),\pm} = \pm \hbar^{-1} \sqrt{2m_e(\mu + E) - \hbar^2 k_y^2 + \alpha^2 m_e^2 k_y^2 / \hbar^2} \mp \alpha m_e k_y / \hbar^2$, in which the \pm sign denotes the propagation direction along the $\pm x$, $e \uparrow (\downarrow)$ describes electron with spin up (down), and $\mp = -(+)$ for $\uparrow (\downarrow)$. Here, we assume translational invariance in the y direction with belonging momentum k_y of the incident particle.

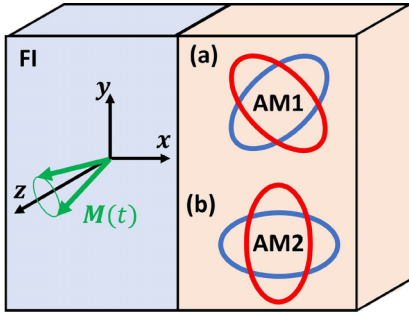


FIG. 1. Spin pumping is considered in a bilayer consisting of a ferromagnetic insulator (FI) and an altermagnet (AM). The magnetization $\mathbf{M}(t)$ in the FI is precessing around the z axis at the FMR frequency Ω . Different interface orientations are also considered, effectively rotating the spin-resolved Fermi surface in the AM for $e \uparrow$ (red ellipse) and $e \downarrow$ (blue ellipse) spin carriers. For notational simplicity, the two AM orientations are referred to as AM1 and AM2, respectively.

On the other hand, the Hamiltonian for the FI has the form

$$H_{\text{FI}} = -\frac{\hbar^2 \nabla^2}{2m_e} + U + J\hat{\sigma} \cdot \mathbf{M}(t), \quad (2)$$

in which $\hat{\sigma}$ denotes the Pauli matrix vector and J is the exchange interaction. Here, the potential U is larger than μ in the nearby AM to ensure the ferromagnet is insulating. The normalized magnetization is defined as $\mathbf{M}(t) = (m \cos \Omega t, m \sin \Omega t, \sqrt{1 - m^2})$, where $m \in [0, 1]$ is the magnetization oscillation amplitude and Ω denotes the FMR frequency for spin pumping. By employing a wave function with the structure $(e^{-\frac{i\Omega t}{2}}, e^{\frac{i\Omega t}{2}})^T$ for its additional time dependence, the nonstationary Schrödinger equation can be solved as an eigenvalue problem (see SM [42] for details). The two eigenpairs are obtained as $E_1 = E_+$ with $(a_+, b_+)^T$ and $E_2 = E_-$ with $(a_-, b_-)^T$, in which $E_{\pm} = U + \frac{\hbar^2(k_x^2 + k_y^2)}{2m_e} \pm JR$ with $R = (1 - 2\beta\sqrt{1 - m^2} + \beta^2)^{1/2}$ and $\beta = \hbar\Omega/2J$.

To study the spin-pumping effect, we first consider an $e \uparrow$ incident electron with excitation energy E from the AM side based on the FI/AM bilayer. The wave functions are given by

$$\begin{aligned} \Psi_{\text{AM}, e\uparrow} &= \begin{bmatrix} 1 \\ 0 \end{bmatrix} e^{ik_{e\uparrow, -}x} + r \begin{bmatrix} 1 \\ 0 \end{bmatrix} e^{ik_{e\uparrow, +}x} \Big] e^{-\frac{iEt}{\hbar}} \\ &+ r' \begin{bmatrix} 0 \\ 1 \end{bmatrix} e^{ik_{e\downarrow, +}x} e^{-\frac{iE't}{\hbar}}, \quad (3) \\ \Psi_{\text{FI}, e\uparrow} &= t \begin{pmatrix} a_+ e^{-\frac{i\Omega t}{2}} \\ b_+ e^{\frac{i\Omega t}{2}} \end{pmatrix} e^{-ik_{\text{FI}, e\uparrow}x} e^{-\frac{iE_1 t}{\hbar}} \\ &+ p \begin{pmatrix} a_- e^{-\frac{i\Omega t}{2}} \\ b_- e^{\frac{i\Omega t}{2}} \end{pmatrix} e^{-ik_{\text{FI}, e\uparrow}x} e^{-\frac{iE_2 t}{\hbar}}, \quad (4) \end{aligned}$$

in which r and r' are coefficients describing reflection without and with spin flip in the AM, respectively, and t and p are transmission coefficients in the FI. To differentiate it from the incident energy E , the energy after the spin flip in the AM due to spin pumping is denoted as E' . By matching

the time dependence of the wave-function components on the AM and FI sides, we obtain $E' = E - \hbar\Omega$ and $E_1 = E_2 = E - \frac{\hbar\Omega}{2}$. In terms of E , the corresponding x components of the two wave vectors in the FI are expressed as $k_{\text{FI}, e\uparrow} = \hbar^{-1} \sqrt{2m_e[E - U - J(R + \beta)] - \hbar^2 k_y^2}$ and $k_{\text{FI}, e\downarrow} = \hbar^{-1} \sqrt{2m_e[E - U + J(R - \beta)] - \hbar^2 k_y^2}$. Note that the wave numbers in the FI possess imaginary values due to a large potential U , ensuring evanescent electron states in the FI. Details of the wave functions induced by an $e \downarrow$ incident particle with excitation energy E from the AM can be found in the SM [42], in which we have $E' = E + \hbar\Omega$.

Appropriate boundary conditions are required to solve the reflection and transmissions coefficients in the wave functions. Here, we consider a Rashba spin-orbit coupled interface with the Hamiltonian

$$H_I = \left[U_0 + \frac{U_{\text{SO}}}{k_F} \hat{\mathbf{x}} \cdot (\hat{\sigma} \times \mathbf{k}) \right] \delta(x) = \left[U_0 - \frac{U_{\text{SO}}}{k_F} k_y \sigma_z \right] \delta(x), \quad (5)$$

in which U_0 is the interfacial energy barrier, U_{SO} describes the Rashba SOC, $k_F = \sqrt{2m_e\mu}/\hbar$ is the Fermi wave vector, and $\hat{\mathbf{x}}$ denotes the interface normal. On the other hand, to derive the boundary condition, antisymmetrization of the altermagnetic term $\alpha k_x k_y \sigma_z \rightarrow \frac{\alpha k_y}{2} \{k_x, \Theta(x)\} \sigma_z$ is necessary to ensure hermiticity of the Hamilton operator, where $\Theta(x)$ is the step function and $k_x = -i\partial_x$. Combining all related Hamiltonian contributions in the FI/AM system, we obtain $\Psi_{\text{AM}, e\uparrow}|_{x=0} = \Psi_{\text{FI}, e\uparrow}|_{x=0} = (f, g)^T$ and

$$\partial_x \Psi_{\text{AM}, e\uparrow}|_{x=0} - \partial_x \Psi_{\text{FI}, e\uparrow}|_{x=0} = \begin{pmatrix} k_{\alpha, +1} f \\ k_{\alpha, -1} g \end{pmatrix}, \quad (6)$$

where $k_{\alpha, \sigma} = \frac{2m_e}{\hbar^2} [U_0 - (\frac{i\alpha}{2} + \frac{U_{\text{SO}}}{k_F}) k_y \sigma]$ with $\sigma = +1(-1)$. Here, the imaginary number i appears in $k_{\alpha, \sigma}$ since we consider k_y invariance (unlike $k_x = -i\partial_x$). Note that the boundary conditions for $e \downarrow$ incident from the AM side have the same forms as $e \uparrow$ with different explicit expressions of f and g in the wave functions.

The longitudinal quantum mechanical spin current polarized along the z axis in the AM is given by

$$j_{sz, e\uparrow(\downarrow)} = \frac{\hbar^2}{2m_e} (\text{Im}\{f^* \nabla f\} - \text{Im}\{g^* \nabla g\}) + \frac{\alpha k_y}{2} (|f|^2 + |g|^2). \quad (7)$$

Integrating over all energies and all possible transverse modes via $\int dk_x = \int dE (dk_x/dE)$ and $\int dk_y$, the spin-pumping current is calculated as

$$I_{s, e\uparrow(\downarrow)} = \int dk_y \int dE \frac{dk_x}{dE} j_{sz, e\uparrow(\downarrow)} f_0(E), \quad (8)$$

in which $f_0(E)$ denotes the Fermi-Dirac distribution. Note that dk_x/dE plays the role of one-dimensional density of states (1D DOS) in the AM instead of 2D DOS since here $\int dk_y$ is included separately. Including contributions from both $e \uparrow$ and $e \downarrow$ incidents, the total spin-pumping current is $I_s = I_{s, e\uparrow} + I_{s, e\downarrow}$. In general, a backflow spin current exists due to a spin accumulation that is built up in the material connected to the precessing FI [1], which diminishes the magnitude of the total spin current flowing across the interface. The backflow spin current can be safely neglected in the

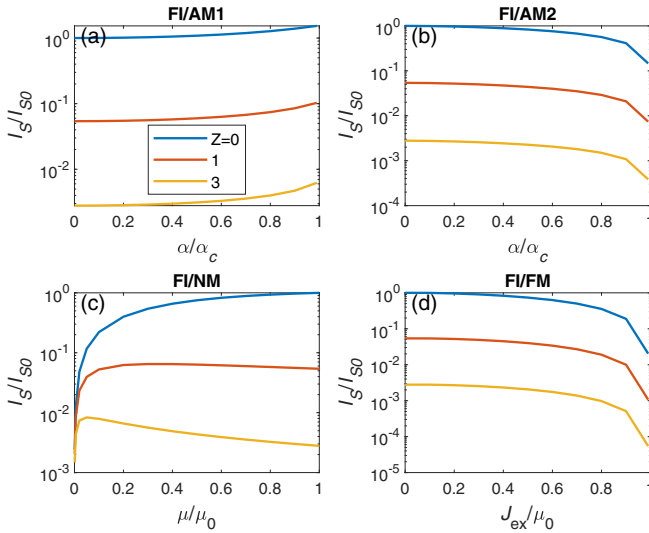


FIG. 2. Normalized spin-pumping current I_s/I_{s0} as a function of altermagnetism for FI/AM1 and FI/AM2 in (a) and (b), respectively. (c) I_s/I_{s0} as a function of chemical potential μ for FI/NM. (d) I_s/I_{s0} as a function of exchange energy J_{ex} for FI/FM. In the absence of Rashba SOC, different interfacial barriers $Z = 0, 1, 3$ are considered. Here, $m = 0.2$ and $\hbar\Omega = 0.5$ meV are utilized. I_{s0} corresponds to the spin-pumping current for FI/NM with $\mu/\mu_0 = 1$.

present case of a ballistic large AM reservoir. To show how the crystallographic orientation of the interface between the materials affects the spin pumping, the AM corresponding to a 45° rotation of the interface, as shown in Fig. 1(b), is modeled by replacing $\alpha k_x k_y \rightarrow \alpha(k_x^2 - k_y^2)/2$ in H_{AM} . This leads to different expressions for the wave vectors, boundary conditions, and quantum mechanical spin-pumping current (see SM [42] for details). Our model can also be expanded to a AM with arbitrary rotation by combination of the established 0° and 45° cases, i.e., using $\alpha_1 k_x k_y \sigma_z + \alpha_2(k_x^2 - k_y^2)\sigma_z/2$ in H_{AM} with the arbitrary angle determined by $\theta_\alpha = \frac{1}{2} \arctan(\alpha_1/\alpha_2)$.

Results: Altermagnetism dependence. For notational simplicity, we refer to the altermagnetic Fermi-surface structures shown in Figs. 1(a) and 1(b) as AM1 and AM2, respectively, corresponding to different interface orientations by effectively rotating 45° of the spin-resolved Fermi surfaces. To ensure each spin-polarized lobe of the altermagnetic Fermi surface described by H_{AM} defines a closed integral path or ellipse rather than a hyperbola, $\alpha < \hbar^2/m_e \equiv \alpha_c$ should be satisfied (see SM [42] for details). The semimajor (minor) axis a (b) of the ellipse can be obtained as

$$a = \sqrt{\frac{2m_e(\mu + E)}{\hbar^2 - m_e\alpha}}, \quad b = \sqrt{\frac{2m_e(\mu + E)}{\hbar^2 + m_e\alpha}}, \quad (9)$$

based on which a (b) increases (decreases) with α .

In the absence of Rashba SOC, the dimensionless parameter $Z = \frac{m_e U_0}{\hbar^2 k_F}$ characterizes the quality of electric contact between the FI and AM. To model high-transparent to tunneling interfaces, we investigate the spin-pumping current I_s with $Z = 0, 1, 3$ in Fig. 2. As is reasonable, I_s decreases as Z increases. More importantly, we find that I_s increases with α in FI/AM1 [Fig. 2(a)] while it decreases with α in

FI/AM2 [Fig. 2(b)], indicating the crucial role of the interface orientation in FI/AM for spin pumping.

To understand the altermagnetism dependence behavior, it is instructional to consider the altermagnetic Fermi surfaces and energy bands. For simplicity, let us focus on particles close to normal incidence, $k_y \rightarrow 0$, which contribute the most to the transport across the junction. In AM1, the wave vectors of the $e \uparrow$ and $e \downarrow$ incident particles are the same, i.e., $k_{e\uparrow(\downarrow),\pm} = \pm \hbar^{-1} \sqrt{2m_e(\mu + E)}$, just as the NM case. This analogy also applies when integrating over all possible k_y values, i.e., the total spin polarization of the incident particles cancels since spin- \downarrow is the majority carrier for $k_y > 0$ and spin- \uparrow is the majority carrier for $k_y < 0$ and the two spin bands contribute equally. On the other hand, in AM2, the wave vectors can be strongly mismatched even for $k_y \rightarrow 0$, i.e., $k_{e\uparrow,\pm} = \pm \hbar^{-1} \sqrt{2m_e(\mu + E)/(\hbar^2 + m_e\alpha)}$ and $k_{e\downarrow,\pm} = \pm \hbar^{-1} \sqrt{2m_e(\mu + E)/(\hbar^2 - m_e\alpha)}$. This is similar to the ferromagnetic metal (FM) case, in which a large mismatch between these wave vectors is induced by a (momentum-independent) spin splitting or exchange energy J_{ex} by considering the Hamiltonian $H_{FM} = -\frac{\hbar^2 \nabla^2}{2m_e} - \mu + J_{ex} \sigma_z$. Therefore, it is useful to compare the spin-pumping current based on FI/NM and FI/FM, as shown in Figs. 2(c) and 2(d), respectively.

The total spin current is determined by the spin-flip probability between $e \uparrow$ and $e \downarrow$ states induced by spin pumping, and also the number of available k_y modes for spin flip. Let us first consider the altermagnetism dependence of the number of k_y modes. As discussed before, a (b) increases (decreases) with α . In AM1, the allowed number of k_y modes or $|k_y|$ maximum for both $e \uparrow$ and $e \downarrow$ bands increases with α as the semimajor axis a increases, giving rise to more available transverse k_y modes in which the spin flip between $e \uparrow$ and $e \downarrow$ can be realized. Note that the symmetry between incident spin $e \uparrow$ and $e \downarrow$ is broken by the spin-pumping FMR frequency Ω . Therefore, the total spin current I_s , which includes contributions from both $e \uparrow$ and $e \downarrow$ incidents, is enhanced when integrating over k_y . This is consistent with the trends shown in Fig. 2(a). Similarly, the allowed k_y range for spin flip can be increased by increasing μ in the NM, giving rise to an enhanced I_s with a high-transparent $Z = 0$ interface [see the blue curve in Fig. 2(c)]. However, it can be seen that the trends change for large Z , indicating a difference between increasing α and μ , although in both cases the number of k_y states that carry spin current increases. This can be explained by considering the spin-flip probability for each k_y mode, which we will get back to.

On the other hand, in AM2, the allowed k_y modes increase with increasing α and semimajor axis a for the $e \uparrow$ band while they decrease with increasing α and decreasing semimajor axis b for the $e \downarrow$ band. This results in an enhanced mismatch between the spin bands at a given value of k_y , and therefore less transverse modes available to realize spin flip between the two bands. This corresponds to the trend that I_s is suppressed with α , as shown in Fig. 2(b). The same mechanism applies for FM in Fig. 2(d), in which the mismatch between available k_y modes for $e \uparrow$ and $e \downarrow$ bands is enhanced with increasing J_{ex} , confirming the similarity between AM2 and FM.

Next, we turn to the spin-flip probability at a fixed k_y , in particular small $|k_y|$ close to normal incidence which

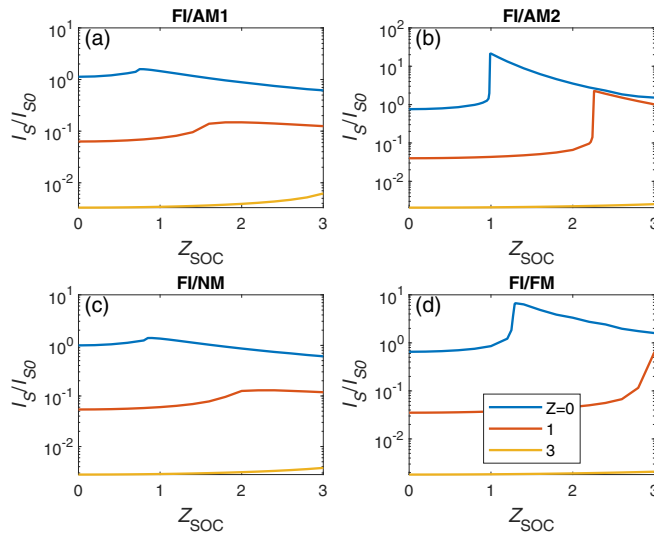


FIG. 3. Normalized spin-pumping current I_s/I_{s0} as a function of Rashba Z_{SOC} for FI/AM1 and FI/AM2 in (a) and (b), respectively, in which $\alpha/\alpha_c = 0.6$. (c) I_s/I_{s0} as a function of Z_{SOC} for FI/NM. (d) I_s/I_{s0} as a function of Z_{SOC} for FI/FM with $J_{\text{ex}}/\mu_0 = 0.6$. Different interfacial barriers $Z = 0, 1, 3$ are considered. Here, $m = 0.2$ and $\hbar\Omega = 0.5$ meV are utilized. I_{s0} corresponds to the spin-pumping current for FI/NM with $\mu/\mu_0 = 1$ in the absence of Rashba SOC, the same as I_{s0} used in Fig. 2.

contribute the most. As calculated in detail in the SM [42] (see Fig. 1 in the SM), it is found that the spin-flip probability increases (decreases) with altermagnetism for FI/AM1 (AM2), which corresponds to the trends shown in Fig. 2. The spin-flip probability behavior can be understood by considering the magnitude of momentum transfer (along x), e.g., when a (spin-flip) reflection requires a large momentum transfer, its probability is diminished [43,44]. In AM1 (AM2), the magnitude of the momentum transfer [e.g., between $k_{e\uparrow,-}$ and $k_{e\downarrow,+}$ in Eq. (3)] at fixed k_y decreases (increases) with altermagnetism. Similarly, in FI/NM, the magnitude of momentum transfer for spin flip increases as μ , which suppresses the spin-flip probability. This compensates the fact that more k_y modes are available when μ increases, as discussed before, giving a total suppression of spin current for large Z in Fig. 2(c).

Results: Spin-orbit dependence. Similar to the barrier $Z = \frac{m_e U_0}{\hbar^2 k_F}$, the interfacial Rashba SOC can be characterized by introducing the dimensionless parameter $Z_{\text{SOC}} = \frac{m_e U_{\text{SOC}}}{\hbar^2 k_F}$, based on which $k_{\alpha,\sigma}$ in Eq. (6) can be written as $k_{\alpha,\sigma} = 2Zk_F - 2Z_{\text{SOC}}k_y\sigma - i\frac{\alpha m_e k_y}{\hbar^2}\sigma$ with $\sigma = +1(-1)$. In Fig. 3, the spin-pumping current is plotted as a function of Z_{SOC} for different bilayers with a gradually increasing interface barrier $Z = 0, 1, 3$. A nonmonotonic behavior with a maximum whose position can be shifted with Z is achieved in all setups. This is related to the effective spin-dependent barrier induced by SOC in the form of $k_y\sigma$ in $k_{\alpha,\sigma}$. When Z_{SOC} is present and Z is

fixed, there exists an optimal value of Z_{SOC} where the barrier is strongly reduced for many angles of incidence (i.e., k_y modes) of a given spin type due to the $k_y\sigma$ dependence in the boundary condition, resulting in enhanced spin flip and spin current. When Z_{SOC} continues to increase, the total barrier then increases again, which causes less spin flip and reduces the spin current. Note that the Fermi-level mismatch between the two layers also results in normal reflection and acts as an effective barrier even when $Z = 0$ [45], which can thus be compensated by Z_{SOC} to achieve the optimal spin current via the argument above.

In the absence of Z_{SOC} , it is shown in Fig. 2 that FI/AM1 produces a larger spin-pumping current compared with FI/AM2, indicating that AM1 is the spin-pumping-enhanced orientation. However, this changes when Z_{SOC} is present. FI/AM2 with the spin-pumping-suppressed orientation can in that case generate a much larger spin current compared with FI/AM1 when Z_{SOC} is tuned to its optimal value, as shown in Fig. 3(b). Similar behavior can be observed in FI/FM [Fig. 3(d)] but with a smaller spin-pumping current maximum compared with FI/AM2. The suppression of spin current due to an interfacial Rashba interaction via spin memory loss and spin-current absorption has been studied previously [28] within a perturbative framework.

Concluding remarks. A YIG/RuO₂ bilayer grown on a gadolinium gallium garnet substrate is suggested to experimentally test our model. This type of structure has been grown to study thermal effects as control samples in Ref. [41] with different RuO₂ crystal orientations and crystalline quantities, giving experimental information about the effect of varying the altermagnetism strength and interface orientation. As for the tuning of interfacial Rashba SOC, this has previously been experimentally demonstrated using a gate voltage [46]. However, it is fair to state that this is probably challenging for the proposed structure, and that the strength of the interfacial SOC might be better accomplished by tailoring the interface properties using, for instance, ultrathin heavy metals such as Pt.

We investigate spin pumping from a FI to an AM by considering two representative AMs with 0° and 45° rotation relative to the interface. We find the spin-pumping current can be both enhanced and suppressed by altermagnetism depending on the interface orientation. In addition, the inclusion of interfacial Rashba SOC strongly affects the spin-pumping current by changing the preferred interface orientation for altermagnetism when the SOC strength is optimized, indicating the crucial role of combining the interface orientation and Rashba SOC for spin pumping in altermagnets.

Acknowledgments. This work was supported by the Research Council of Norway through Grant No. 323766 and its Centres of Excellence funding scheme Grant No. 262633 “QuSpin.” Support from Sigma2 - the National Infrastructure for High Performance Computing and Data Storage in Norway, Project No. NN9577K, is acknowledged.

[1] Y. Tserkovnyak, A. Brataas, G. E. W. Bauer, and B. I. Halperin, *Rev. Mod. Phys.* **77**, 1375 (2005).

[2] Y. Tserkovnyak, A. Brataas, and G. E. W. Bauer, *Phys. Rev. B* **66**, 224403 (2002).

- [3] Y. Tserkovnyak, A. Brataas, and G. E. W. Bauer, *Phys. Rev. Lett.* **88**, 117601 (2002).
- [4] A. Brataas, B. van Wees, O. Klein, G. de Loubens, and M. Viret, *Phys. Rep.* **885**, 1 (2020).
- [5] C. Sun, H. Yang, and M. B. A. Jalil, *Phys. Rev. B* **105**, 104407 (2022).
- [6] C. Sun, H. Yang, A. Brataas, and M. B. A. Jalil, *Phys. Rev. Appl.* **17**, 034028 (2022).
- [7] B. Heinrich, C. Burrowes, E. Montoya, B. Kardasz, E. Girt, Y.-Y. Song, Y. Sun, and M. Wu, *Phys. Rev. Lett.* **107**, 066604 (2011).
- [8] M. Haertinger, C. H. Back, J. Lotze, M. Weiler, S. Geprägs, H. Huebl, S. T. B. Goennenwein, and G. Woltersdorf, *Phys. Rev. B* **92**, 054437 (2015).
- [9] F. Yang and P. C. Hammel, *J. Phys. D: Appl. Phys.* **51**, 253001 (2018).
- [10] S. M. Rezende, R. L. Rodríguez-Suárez, M. M. Soares, L. H. Vilela-Leão, D. Ley Domínguez, and A. Azevedo, *Appl. Phys. Lett.* **102**, 012402 (2013).
- [11] V. Castel, N. Vlietstra, B. J. van Wees, and J. B. Youssef, *Phys. Rev. B* **86**, 134419 (2012).
- [12] C. Sun and J. Linder, *Phys. Rev. B* **107**, 144504 (2023).
- [13] K.-R. Jeon, C. Ciccarelli, A. J. Ferguson, H. Kurebayashi, L. F. Cohen, X. Montiel, M. Eschrig, J. W. A. Robinson, and M. G. Blamire, *Nat. Mater.* **17**, 499 (2018).
- [14] Y. Yao, Q. Song, Y. Takamura, J. P. Cascales, W. Yuan, Y. Ma, Y. Yun, X. C. Xie, J. S. Moodera, and W. Han, *Phys. Rev. B* **97**, 224414 (2018).
- [15] S. J. Carreira, D. Sanchez-Manzano, M.-W. Yoo, K. Seurre, V. Rouco, A. Sander, J. Santamaría, A. Anane, and J. E. Villegas, *Phys. Rev. B* **104**, 144428 (2021).
- [16] M. Inoue, M. Ichioka, and H. Adachi, *Phys. Rev. B* **96**, 024414 (2017).
- [17] T. Kato, Y. Ohnuma, M. Matsuo, J. Rech, T. Jonckheere, and T. Martin, *Phys. Rev. B* **99**, 144411 (2019).
- [18] Y. Ominato, A. Yamakage, T. Kato, and M. Matsuo, *Phys. Rev. B* **105**, 205406 (2022).
- [19] Y. Ominato, A. Yamakage, and M. Matsuo, *Phys. Rev. B* **106**, L161406 (2022).
- [20] K.-H. Ahn, A. Hariki, K.-W. Lee, and J. Kuneš, *Phys. Rev. B* **99**, 184432 (2019).
- [21] S. Hayami, Y. Yanagi, and H. Kusunose, *J. Phys. Soc. Jpn.* **88**, 123702 (2019).
- [22] L. Šmejkal, R. González-Hernández, T. Jungwirth, and J. Sinova, *Sci. Adv.* **6**, eaaz8809 (2020).
- [23] L.-D. Yuan, Z. Wang, J.-W. Luo, E. I. Rashba, and A. Zunger, *Phys. Rev. B* **102**, 014422 (2020).
- [24] L. Šmejkal, J. Sinova, and T. Jungwirth, *Phys. Rev. X* **12**, 040501 (2022).
- [25] L. Šmejkal, J. Sinova, and T. Jungwirth, *Phys. Rev. X* **12**, 031042 (2022).
- [26] I. Mazin and The PRX Editors, *Phys. Rev. X* **12**, 040002 (2022).
- [27] I. I. Mazin, *Phys. Rev. B* **107**, L100418 (2023).
- [28] K. Chen and S. Zhang, *Phys. Rev. Lett.* **114**, 126602 (2015).
- [29] L. Šmejkal, A. Marmodoro, K.-H. Ahn, R. Gonzalez-Hernandez, I. Turek, S. Mankovsky, H. Ebert, S. W. D'Souza, O. Šipr, J. Sinova, and T. Jungwirth, [arXiv:2211.13806](https://arxiv.org/abs/2211.13806).
- [30] O. Fedchenko, J. Minar, A. Akashdeep, S. W. D'Souza, D. Vasilyev, O. Tkach, L. Odenbreit, Q. L. Nguyen, D. Kutnyakhov, N. Wind, L. Wenthaus, M. Scholz, K. Rossnagel, M. Hoesch, M. Aeschlimann, B. Stadtmueller, M. Klauui, G. Schoenhense, G. Jakob, T. Jungwirth *et al.*, [arXiv:2306.02170](https://arxiv.org/abs/2306.02170).
- [31] A. Hariki, T. Yamaguchi, D. Kriegner, K. W. Edmonds, P. Wadley, S. S. Dhesi, G. Springholz, L. Šmejkal, K. Výborný, T. Jungwirth, and J. Kuneš, [arXiv:2305.03588](https://arxiv.org/abs/2305.03588).
- [32] C. Sun, A. Brataas, and J. Linder, *Phys. Rev. B* **108**, 054511 (2023).
- [33] J. A. Ouassou, A. Brataas, and J. Linder, *Phys. Rev. Lett.* **131**, 076003 (2023).
- [34] S.-B. Zhang, L.-H. Hu, and T. Neupert, [arXiv:2302.13185](https://arxiv.org/abs/2302.13185).
- [35] M. Papaj, *Phys. Rev. B* **108**, L060508 (2023).
- [36] C. W. J. Beenakker and T. Vakhstel, *Phys. Rev. B* **108**, 075425 (2023).
- [37] Z. Jin, H. Yang, Z. Zeng, Y. Cao, and P. Yan, [arXiv:2307.00909](https://arxiv.org/abs/2307.00909).
- [38] J. Ren, X. Chen, Y. Zhu, Y. Yu, A. Zhang, J. Li, Y. Liu, C. Li, and Q. Liu, [arXiv:2307.10369](https://arxiv.org/abs/2307.10369).
- [39] S. Das, D. Suri, and A. Soori, *J. Phys.: Condens. Matter* **35**, 435302 (2023).
- [40] Y. Jiang, Z. Song, T. Zhu, Z. Fang, H. Weng, Z.-X. Liu, J. Yang, and C. Fang, [arXiv:2307.10371](https://arxiv.org/abs/2307.10371).
- [41] H. Bai, Y. C. Zhang, Y. J. Zhou, P. Chen, C. H. Wan, L. Han, W. X. Zhu, S. X. Liang, Y. C. Su, X. F. Han, F. Pan, and C. Song, *Phys. Rev. Lett.* **130**, 216701 (2023).
- [42] See Supplemental Material at <http://link.aps.org/supplemental/10.1103/PhysRevB.108.L140408> for derivation details.
- [43] X.-T. An, J. Xiao, M. W.-Y. Tu, H. Yu, V. I. Fal'ko, and W. Yao, *Phys. Rev. Lett.* **118**, 096602 (2017).
- [44] J.-H. Guan, Y.-Y. Zhang, S.-S. Wang, Y. Yu, Y. Xia, and S.-S. Li, *Phys. Rev. B* **102**, 064203 (2020).
- [45] G. E. Blonder and M. Tinkham, *Phys. Rev. B* **27**, 112 (1983).
- [46] E. Lesne, Y. Fu, S. Oyarzun, J. C. Rojas-Sánchez, D. C. Vaz, H. Naganuma, G. Sicoli, J.-P. Attané, M. Jamet, E. Jacquet, J.-M. George, A. Barthélémy, H. Jaffrès, A. Fert, M. Bibes, and L. Vila, *Nat. Mater.* **15**, 1261 (2016).